Improvements in bottomside electron density definition in the Autoscala program

C. Scotto[(1)], D. Sabbagh[(2)]

Istituto Nazionale di Geofisica e Vulcanologia, Via di Vigna Murata 605, 00143 Rome, Italy

[(1)] carlo.scotto@ingv.it, [(2)] dario.sabbagh@ingv.it

Abstract

Some improvements introduced in the Autoscala program are presented. They include improvements in E valley modeling of the electron density profile $N_e(h)$, and in the link between the E valley and bottom-side F regions. An abrupt variation in $N_e(h)$ generated by the previous version of Autoscala under night conditions has been eliminated.

A series of ionograms recorded by the Millstone Hill digisonde (42.6°, 288.5°) were automatically interpreted by the previous version of Autoscala and by the new one. Data from Incoherent Scatter Radar (ISR) were used to comparatively assess the performance of the two versions. For this purpose, the root mean square errors (*RMSE*s) of the $N_e(h)$ provided by Autoscala were calculated relative to the corresponding values provided by ISR.

A more accurate overall modeling of $N_e(h)$ was achieved by the new Autoscala version (*RMSE* = 0.51 MHz for the new version against *RMSE* = 0.67 MHz for the previous one).

1. Introduction

Autoscala is a computer program developed at the INGV (Istituto Nazionale di Geofisica e Vulcanologia), for the automatic scaling of the critical frequency foF2 and the Maximum Usable Frequency MUF(3000)F2 from ionograms (Scotto and Pezzopane, 2002; Pezzopane and Scotto, 2004, 2005, 2007). Autoscala was extended with the implementation of a routine for the automatic scaling of the sporadic-E layer (Scotto and Pezzopane, 2007) and a routine for the F1 layer (Pezzopane and Scotto, 2008). It works by applying analytical empirical functions to match the typical asymptotic shape of the ionogram traces and detect the F1 and F2 layers. The matching procedure is performed using an image recognition technique, which allows the software to operate without polarization information. The software was originally designed to be used with the AIS-INGV (Advanced Ionospheric Sounder) developed at the INGV, but it can be used with any ionosonde (Bullett et al., 2010; Pezzopane et al., 2010).

Subsequently, a method to obtain the vertical electron density profile $N_e(h)$ was implemented in Autoscala and has now become an integral part (Scotto, 2009). The algorithm operates on the basis of an $N_e(h)$ model (the Adaptive Ionospheric Profiler, AIP), based on 12 free parameters p_1, p_2, ..., p_{12} from which an $N_e(h)$ can be estimated. The parameters p_i (with i=1,….,12) of the model are then varied across appropriate ranges I_1, I_2, ..., I_{12} in the neighborhood of certain $p_{i[base]}$ values. These are referred to as "base values" and modeled according to the helio-geophysical condition and the results of an image recognition procedure, applied by Autoscala to the ionogram to detect the ionospheric characteristics (Scotto and Pezzopane, 2002; Pezzopane and Scotto, 2004, 2005, 2007; Scotto and Pezzopane, 2007; Pezzopane and Scotto, 2008). In this way a wide set of profiles are obtained and, based on these, a corresponding set of artificial ionograms. Among these, the algorithm is able to select the ionogram that best approximates the recorded one.

Reference is made to the articles mentioned above and in particular to the one by Scotto (2009) describing AIP and the procedure it applies to select $N_e(h)$, generating a corresponding restored ionogram trace. This article describes the main changes that have recently been introduced into Autoscala. They concern the modeling of the E-region and the link between the bottom-side F and E regions. For convenience in the following the previous version will be indicated as Autoscala-2007 and the version being introduced in this article as Autoscala-2018.

2. Modeling the E-region

A sketch of the $N_e(h)$ model used by AIP is reported in Fig. 1. The model is based on the definition of six anchor points, which are reported in Fig. 1 as A, B, C, D, E, and F.
In Autoscala-2007 the D point was modeled applying the Mahajan et al. (1997) formulation for h_vE, N_mE and δN_vE. Instead, in this version the D point is modeled assuming the same formulation as in the IRI model (Bilitza et al., 2017). h_vE is then computed with:

$$h_vE=h_mE+h_{deep}E, \quad (1)$$

where h_mE=110 km, $h_{deep}E=10.5/\Delta$ for daytime and $h_{deep}E$=28 km for nighttime. The value of Δ is set to 4.32 if $|modip|<18$ and to $1+\exp[-(|modip|-30)/10]$ otherwise, where *modip* is a modified magnetic dip angle proposed by Rawer (1963).
Concerning the electron density of point D, this is computed starting from the depth percentage $\delta N_v\%$ of the valley. From this, δN_vE is computed as:

$$\delta N_vE = N_mE \cdot \delta N_v\%/100, \quad (2)$$

where $\delta N_v\%=10/\Delta$ for winter daytime, $\delta N_v\%=5/\Delta$ for other seasons daytime, and $\delta N_v\%$=81 for nighttime. A procedure for smooth time interpolation is used for both $\delta N_v\%$ and $h_{deep}E$ (Bilitza et al., 1990). The day-night transition function used is a combination of two Epstein step functions and varies with local time continuously from a constant nighttime value to a constant daytime value. The steps occur at the local times of sunrise and sunset, and the step width is set to one hour.

3. Link between the bottom-side F and E region profiles

Referring again to Fig. 1, it can be noted that the $N_e(h)$ model applied in this work can be divided into the following two regions:

1) the bottom-side F2 profile, through the F1 layer to the top of the E valley (from A to C, in Fig. 1);

2) the E region (from C to F, in Fig. 1).

The bottom-side F2 profile is defined on the basis of the F1 layer formulation in the IRI $N_e(h)$ from Reinisch and Huang (2000). A is the fundamental anchor point, and the E region is modeled by defining the position of the four anchor points C, D, E, and F (see Fig. 1), which are joined by polynomial functions (Scotto, 2009).

Here it is important to observe the criticality of the connection between the regions 1) and 2) mentioned above, which occurs at point C. In Autoscala-2007, point C was first defined, once the electron density N_mE and height $h_mE+\delta h_vE$ are specified. Then, the parabolic connection between C and D was established, and finally the passage of the Reinisch and Huang (2000) function was required for point C. The parabola joining C to the point D was calculated by requiring a vertical slope at D, and continuity at points D and C. Since no constraint was imposed on the first derivative in C, here a discontinuity was generated. In order to remove such a first derivative discontinuity a third order polynomial had been introduced between two points C_1 and C_2 located 3 km above and below C. The coefficients of this polynomial had been computed requiring the continuity of the first derivative in C_1 and C_2. Although this artifice allowed for a continuous first derivative, it underwent sudden variation of $N_e(h)$ over a range of a few kilometers around C. This abrupt variation is evident in nocturnal conditions when the depth of the modeled valley is extremely modest (Fig. 2b and Fig. 3b).

In the version presented here, the algorithm operates in a different way: first the passage of the Reinisch and Huang (2000) function is imposed for C. Then, points C and D are connected with a function whose parameters are chosen to have continuous first derivative in C and vertical trend in D. The function used is of the type:

$$N_e(h)=(N_mE-\delta N_v)+\delta N_v\cdot[(h-h_vE)/(h_mE+\delta h_vE-h_vE)]^{\alpha}. \quad (3)$$

This function guarantees that $N_e(h)$ has a vertical tangent at the point D ($h=h_vE$). The continuity of the first derivative in C ($h=h_mE+\delta h_vE$) is obtained by imposing:

$$\alpha=[dN_e(h)/dh]_{h=h_mE+\delta h_vE}\cdot(h_mE+\delta h_vE-h_vE)/\delta N_v, \quad (4)$$

where $[dN_e(h)/dh]_{h=h_mE+\delta h_vE}$ is the derivative of the Reinisch and Huang (2000) function computed in C.

4. Comparison with data from Incoherent Scatter Radar

536 ionograms recorded in the period from January 2010 to December 2017 by the digisonde installed at Millstone Hill (42.6°, 288.5°) were considered, with almost simultaneous profiles $N_e(h)_{ISR}$ recorded by the colocated Incoherent Scatter Radar (ISR). The considered ionograms were those for which the critical frequency f_oF2 provided by Autoscala matched the one observed by ISR, in order to not affect the analysis by cases of wrong f_oF2 autoscaling. In this way the root mean square errors (*RMSE*s) for h between 110 km and h_mF2:

$$RMSE_{Autoscala2018}=\sqrt{\sum_{i=1}^{n}\frac{[f_p(h)_{[ISR]i}-f_p(h)_{[Autoscala2018]i}]^2}{n}}, \quad (5)$$

and

$$RMSE_{Autoscala2007}=\sqrt{\sum_{i=1}^{n}\frac{[f_p(h)_{[ISR]i}-f_p(h)_{[Autoscala2007]i}]^2}{n}}, \quad (6)$$

are representative only of the differences in the profiles shape, with the symbol meanings being self-evident. The study was carried out considering nocturnal and diurnal conditions separately.

Fig. 2(a-b) shows a comparison between the Autoscala-2018 version and the previous one, for a nighttime ionogram recorded at Millstone Hill on June 10, 2011 at 04.45 UT. The data from ISR are used as an independent measure to compare the performance of the two different Autoscala versions. In this case the result was $RMSE_{Autoscala2018}$=0.16 MHz and $RMSE_{Autoscala2007}$=0.35 MHz. Fig. 3(a)-(b) shows another comparison of Autoscala-2018 with Autoscala-2007, for a nighttime ionogram recorded at Millstone Hill on January 18, 2013 at 05.15 UT. In this case the result was $RMSE_{Autoscala2018}$=0.23 MHz and $RMSE_{Autoscala2007}$=0.18 MHz.

The example reported in Fig. 4(a)-(b) refers to a diurnal ionogram, recorded at Millstone Hill on January 23, 2010 at 20.15 UT. In this case the result was $RMSE_{Autoscala2018}$=0.15 MHz and $RMSE_{Autoscala2007}$=0.70 MHz.

Fig. 5 shows the plot of $RMSE_{Autoscala2018}$ and $RMSE_{Autoscala2007}$ for night and day ionograms. The values computed over all the diurnal available ionograms were $RMSE_{Autoscala2018}$=0.58 MHz and $RMSE_{Autoscala2007}$=0.83 MHz. Considering all the available nighttime ionograms gave values of

$RMSE_{\text{Autoscala2018}}$=0.43 MHz and of $RMSE_{\text{Autoscala2007}}$=0.47 MHz. The diurnal, nocturnal, and overall results obtained are reported in Table 1.

5. Conclusions

Regarding nighttime ionograms, Autoscala-2018 eliminates the abrupt variation of $N_e(h)$ produced by Autoscala-2007 at the connection between the E valley and the intermediate region. This improved behavior can be seen by comparing Fig. 2(a) with Fig. 2(b) and Fig. 3(a) with Fig. 3(b). These figures show examples of systematic behavior. However, there are cases like the one shown in Fig. 2(a)-(b), in which $RMSE_{\text{Autoscala2007}} > RMSE_{\text{Autoscala2018}}$, but also cases like the one shown in Fig. 3(a)-(b), in which $RMSE_{\text{Autoscala2007}} < RMSE_{\text{Autoscala2018}}$. As a consequence, for nighttime ionograms as a whole, Autoscala-2018 provides only slightly better accuracy in the estimation of $N_e(h)$ than the one provided by Autoscala-2007 ($RMSE_{\text{Autoscala2018}}$=0.43 MHz and $RMSE_{\text{Autoscala2007}}$=0.47 MHz).

Regarding daytime ionograms, Autoscala-2018 provides a more accurate estimate of $N_e(h)$ compared to Autoscala-2007. A clear example of this is shown in Fig. 4(a)-(b). In this case $RMSE_{\text{Autoscala2007}}$=0.70 MHz and $RMSE_{\text{Autoscala2018}}$=0.15 MHz. This behavior is reasonably systematic, so that for diurnal ionograms overall, it emerges that $RMSE_{\text{Autoscala2018}}$=0.58 MHz and $RMSE_{\text{Autoscala2007}}$=0.83 MHz.

The results obtained for daytime and nighttime ionograms together ($RMSE_{\text{Autoscala2018}}$=0.51 MHz and $RMSE_{\text{Autoscala2007}}$=0.67 MHz), show that, in terms of the bottomside electron density representation, Autoscala-2018 behaves better than Autoscala-2007, at least at mid latitudes.

6. Acknowledgements

Radar observations and analysis at Millstone Hill and Madrigal distributed database services are supported by US National Science Foundation Cooperative Agreement AGS-1242204 with the Massachusetts Institute of Technology.

Millstone Hill ionograms have been downloaded from the DIDB, Center for Atmospheric Research, University of Massachusetts, Lowell.

7. References

Bilitza, D., Rawer, K, Bossy, L., Kutiev, I., Oyama, K.-I., Leitinger, R., Kazimirovsky, E. International Reference Ionosphere 1990, NSSDC 90-22, Greenbelt, Maryland, 1990. [PDF1: pages 0-84, PDF2: pages 85-end].

Bilitza, D., Altadill, D., Truhlik, V., Shubin, V., Galkin, I., Reinisch, B., Huang, X., 2017. International Reference Ionosphere 2016: From ionospheric climate to real-time weather predictions. Space Weather 15, 418–429, doi:10.1002/2016SW001593.

Bullett, T., Malagnini, A., Pezzopane, M., Scotto, C., 2010. Application of Autoscala to ionograms recorded by the VIPIR ionosonde, Adv. Space Res. 45 (9), 1156-1172.

Mahajan, K.K, Sethi, N.K, Pandey, V.K., 1997. The diurnal variation of E-F valley parameters from Incoherent Scatter measurements at Arecibo. Adv. Space Res. 20, 1781-1784.

Pezzopane, M., Scotto, C., 2004. Software for the automatic scaling of critical frequency foF2 and MUF(3000)F2 from ionograms applied at the Ionospheric Observatory of Gibilmanna. Ann. Geophys. 47, 1783–1790.

Pezzopane, M., Scotto, C., 2005. The INGV software for the automatic scaling of foF2 and MUF(3000)F2 from ionograms: a performance comparison with ARTIST 4.01 from Rome data. J. Atmos. Solar-Terr. Phys. 67, 1063–1073.

Pezzopane, M., Scotto, C., 2007. The automatic scaling of critical frequency foF2 and MUF(3000)F2: a comparison between Autoscala and ARTIST 4.5 on Rome data. Radio Sci. 42, RS4003, doi:10.1029/2006RS003581.

Pezzopane, M., Scotto, C., 2008. A method for automatic scaling of F1 critical frequency from ionograms. Radio Sci. 43, RS2S91, doi:10.1029/ 2007RS003723.

Pezzopane, M., Scotto, C., Tomasik, Ł., Krasheninnikov, I., 2010. Autoscala: an aid for different ionosondes, Acta Geophysica 58 (3), 513-526.

Rawer, K., 1963. Propagation of decametric waves (HF- band), in meteorological and Astronomical Influences on Radio Wave Propagation, edited by B. Landmark (New York Academic Press), pp. 221-250.

Reinisch, B.W., Huang, X., 2000. Redefining the IRI F1 layer profile. Adv. SpaceRes. 25, 81–88.

Scotto, C., 2009. Electron density profile calculation technique for Autoscala ionogram analysis. Adv. Space Res., 44, 756-766.

Scotto, C., Pezzopane, M. A software for automatic scaling of foF2 and MUF(3000)F2 from ionograms. Proceedings of URSI 2002, Maastricht, 17–24 August, 2002 (on CD).

Scotto, C., Pezzopane, M., 2007. A method for automatic scaling of sporadic E layers from ionograms. Radio Sci. 42, RS2012, doi:10.1029/2006RS003461.

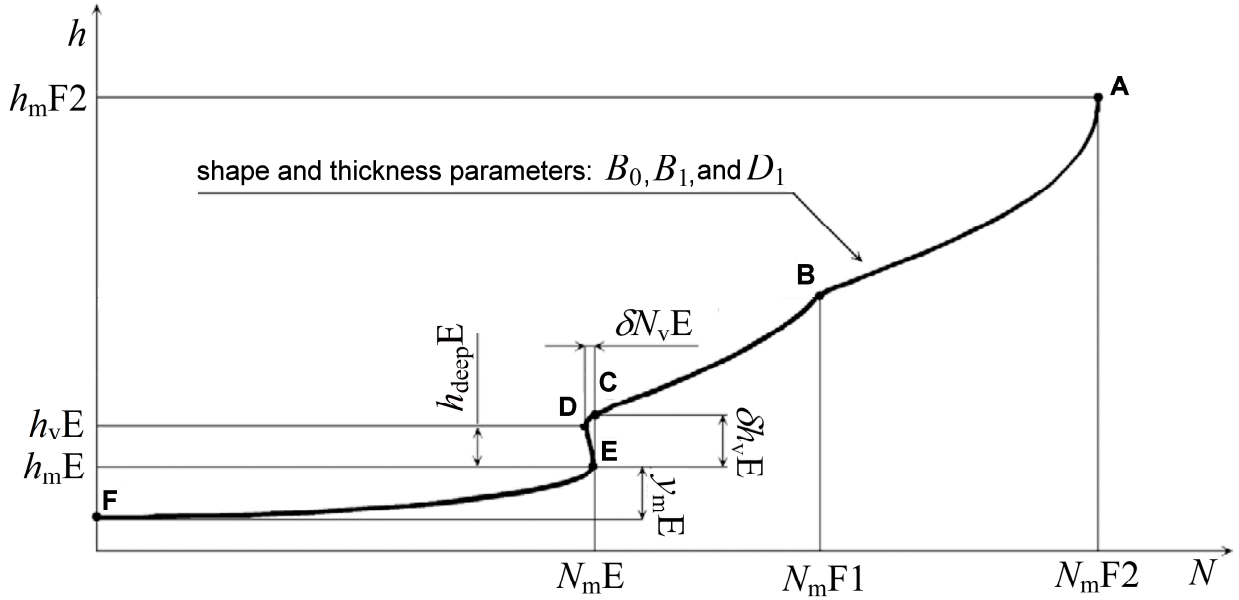

Fig. 1. The electron density profile model used in Autoscala. It can be divided in the following two regions: (1) the bottom-side F2 profile, through the F1 layer down to the top of the E valley (from A to C); (2) the E valley and the E bottomside (from C to F). The parameters used to define region (1) are the shape and thickness parameters B_0, B_1, and D_1, and the peak densities N_mF1 and N_mF2 of the F1 and F2 layers respectively. The parameters used to define region (2) are the peak density N_mE of the E layer, its altitude h_mE, the width and the depth of the E region valley δh_vE and δN_vE respectively, the altitude of the E valley point h_vE, the difference h_{deep}E between the latter and h_mE, and the difference y_mE between h_mE and the altitude of the base of the ionosphere.

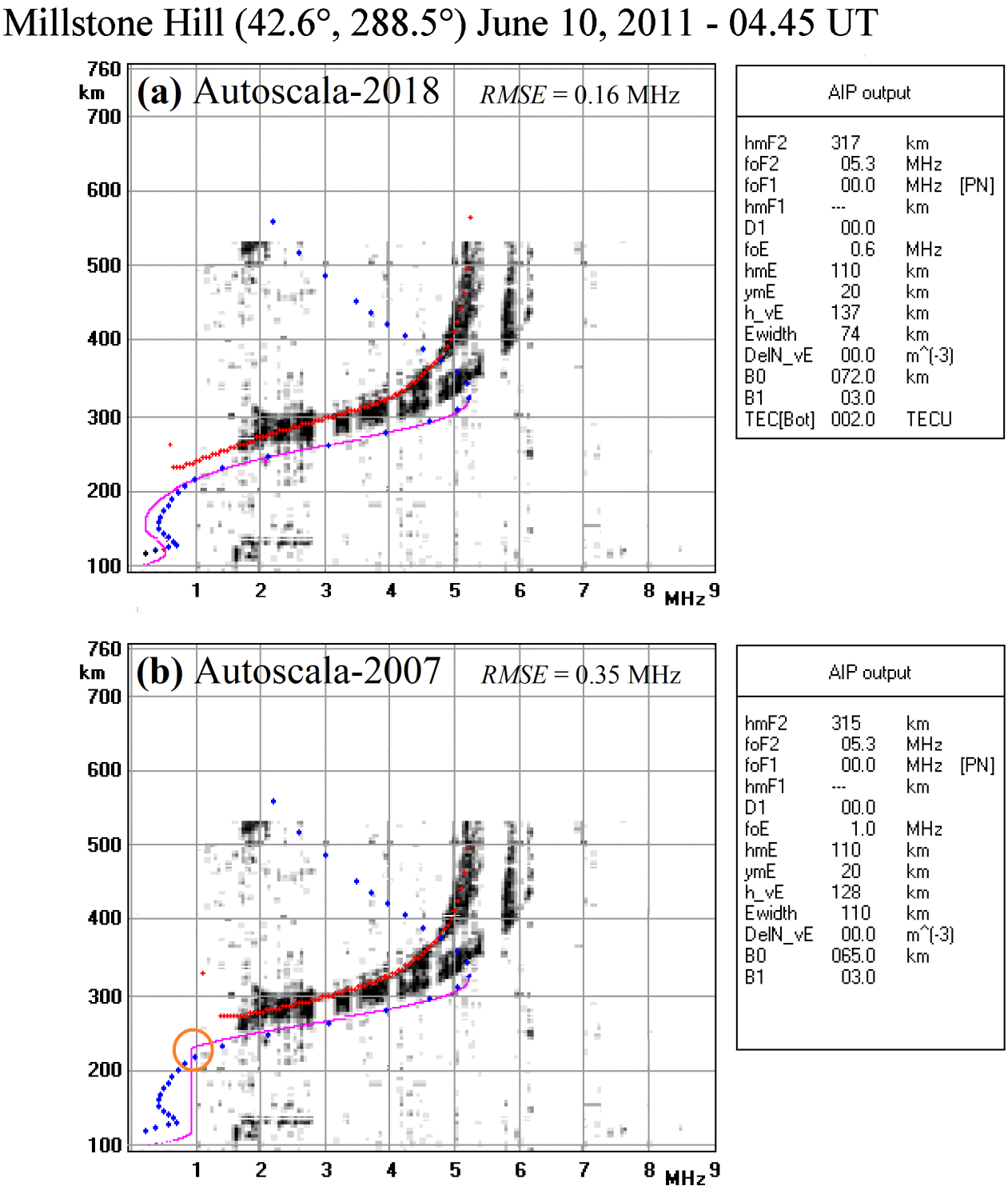

Fig 2. Ionogram recorded at Millstone Hill on June 10, 2011 at 04.45 UT: behavior of (a) Autoscala-2018 compared to (b) Autoscala-2007. The blue curve is the profile recorded by the Incoherent Scatter Radar, while the violet one is the bottomside profile obtained by Autoscala applied to the ionogram. The red line is the synthetic ionogram restored by Autoscala in the autoscaling process. In the new version, the abrupt variation of $N_e(h)$ is eliminated and a more accurate modeling of $N_e(h)$ is achieved, which is confirmed by a lower *RMSE* ($RMSE_{Autoscala2018}$=0.16 MHz against $RMSE_{Autoscala2007}$=0.35 MHz). The abrupt variation of $N_e(h)$ occurring in the old version is highlighted with an orange circle in (b).

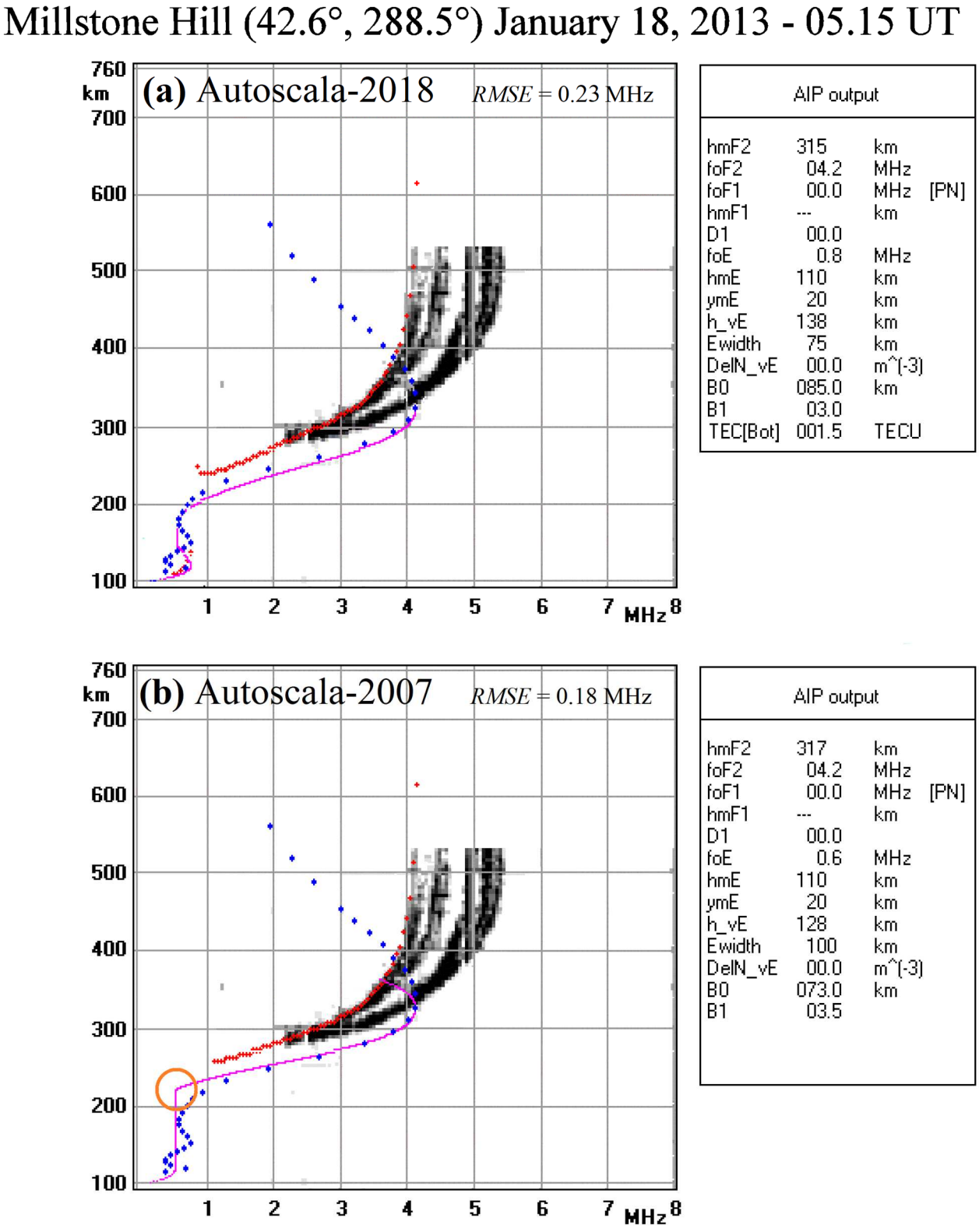

Fig 3. Ionogram recorded at Millstone Hill on January 18, 2013 at 05.15 UT: behavior of (a) Autoscala-2018 compared to (b) Autoscala-2007. The blue curve is the profile recorded by the Incoherent Scatter Radar, while the violet one is the profile obtained by Autoscala applied to the ionogram. The red line is the synthetic ionogram restored by Autoscala in the autoscaling process. In the new version, the abrupt variation of $N_e(h)$ is eliminated. In this case the modeling of $N_e(h)$ is worse, which is confirmed by a higher *RMSE*

($RMSE_{Autoscala2018}$=0.23 MHz, against $RMSE_{Autoscala2007}$=0.18 MHz). The abrupt variation of $N_e(h)$ occurring in the old version is highlighted with an orange circle in (b).

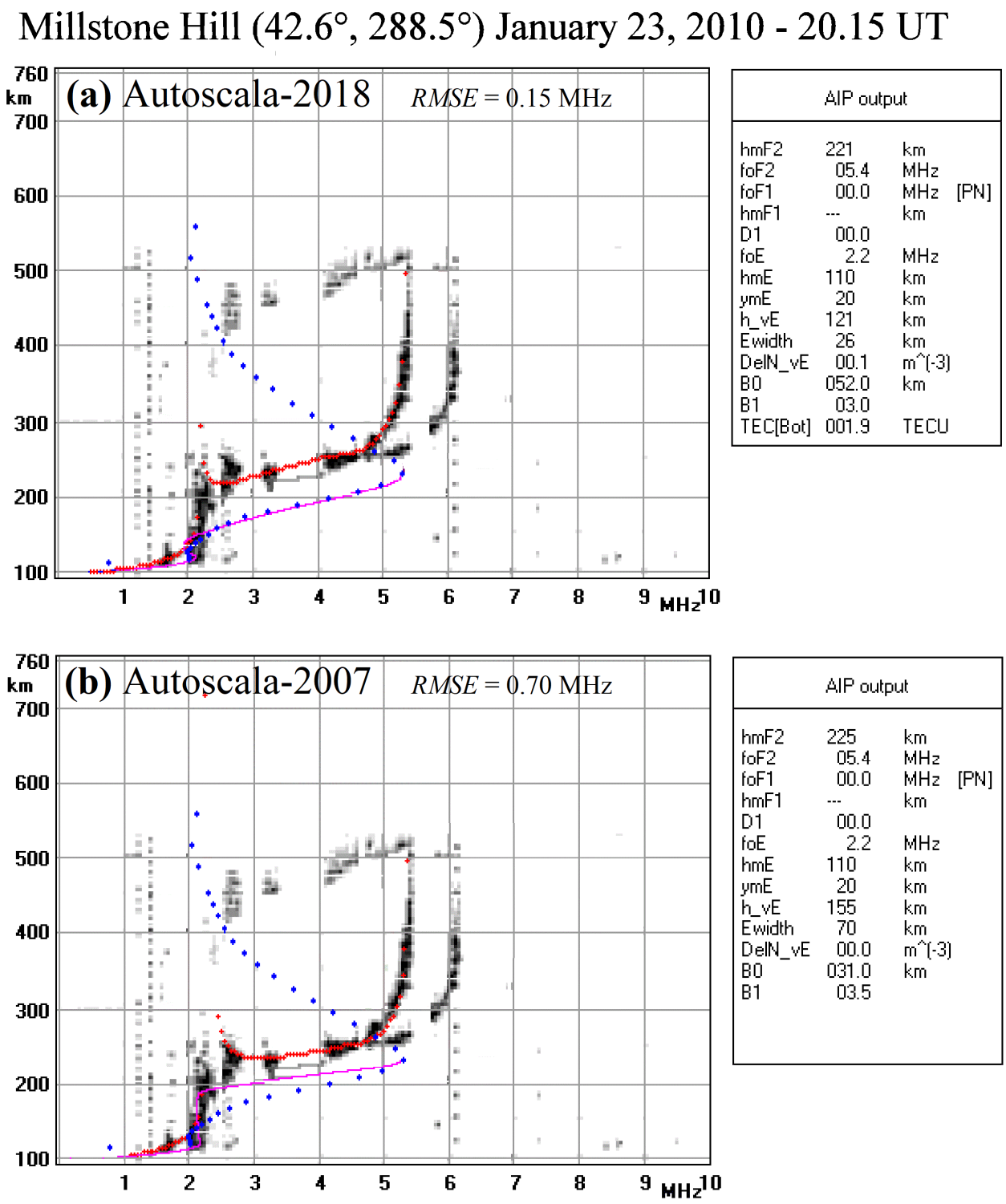

Fig. 4. Ionogram recorded at Millstone Hill on January 23, 2010. The comparison, in daytime conditions, of the behavior of (a) Autoscala-2018 compared to (b) Autoscala-2007. The blue curve is the profile recorded by the Incoherent Scatter Radar, while the violet one is the bottomside profile obtained by Autoscala applied to the ionogram. The red line is the synthetic ionogram restored by Autoscala in the autoscaling process. The

new Autoscala version shows a more accurate modeling of $N_e(h)$, which is confirmed by a lower *RMSE* ($RMSE_{Autoscala2018}$=0.15 MHz, against $RMSE_{Autoscala2007}$=0.70 MHz).

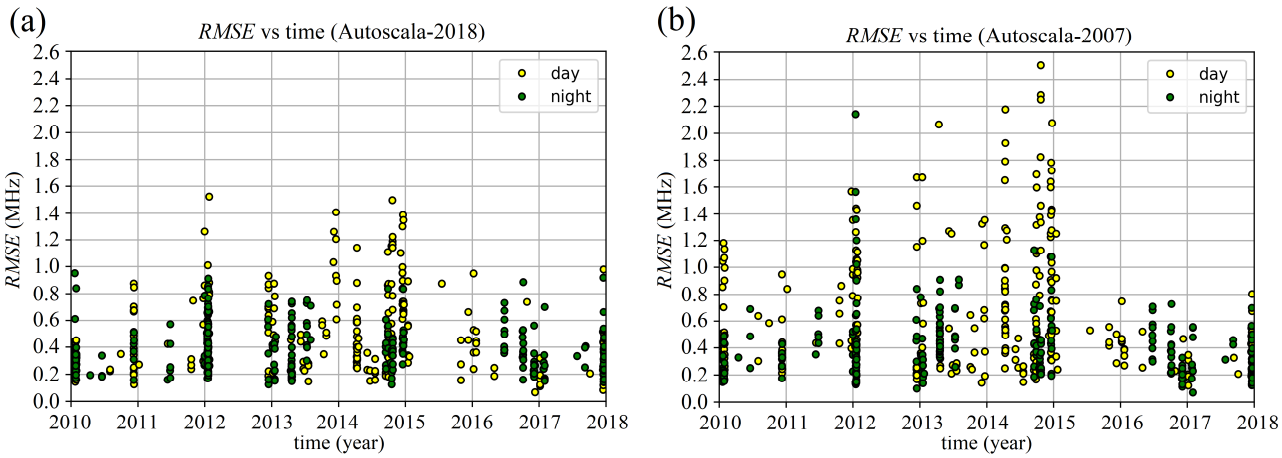

Fig. 5. *RMSE*s values versus time from January 2010 to December 2017 separating day and night conditions for Autoscala-2018 (a) and Autoscala-2007 (b).

Table 1. Comparison between the values of $RMSE_{Autoscala2018}$ and of $RMSE_{Autoscala2007}$ in nighttime and daytime conditions.

	N° of ionograms	$RMSE_{Autoscala2018}$ (MHz)	$RMSE_{Autoscala2007}$ (MHz)
Nighttime	288	0.43	0.47
Daytime	246	0.58	0.83
Overall	534	0.51	0.67